A Level Set Approach to a Unified Model for Etching, Deposition, and Lithography III: Re-Deposition, Re-Emission, Surface Diffusion, and Complex Simulations*

D. Adalsteinsson and J.A. Sethian †

Department of Mathematics
and
Lawrence Berkeley Laboratory
University of California, Berkeley, California 94720

Submitted: Dec. 20, 1996, Journal of Computational Physics, 1996

Abstract

Previously, Adalsteinsson and Sethian have applied the level set formulation to the problem of surface advancement in two and three-dimensional topography simulation of deposition, etching, and lithography processes in integrated circuit fabrication. The level set formulation is based on solving a Hamilton-Jacobi type equation for a propagating level set function, using techniques borrowed from hyperbolic conservation laws. Topological changes, corner and cusp development, and accurate determination of geometric properties such as curvature and normal direction are naturally obtained in this setting. Part I presented the basic equations and algorithms for two dimensional simulations, including the effects of isotropic and uni-directional deposition and etching, visibility, reflection, and material dependent etch/deposition rates. Part II focused on the extension to three dimensions. This paper completes the series, and add the effects of re-deposition, re-emission, and surface diffusion. This requires the solution of the transport equations for arbitrary geometries, and leads to simulations that contain multiple simultaneous competing effects of visibility, directional and source flux functions, complex sputter yield flux functions, wide ranges of sticking coefficients for the re-emission and re-deposition functions, multi-layered triple points and thin film layers.

*Correct citation: Adalsteinsson, D., and Sethian, J.A., J. Comp. Phys., 138, 1, pp. 193-223, 1997.

†Supported in part by the Applied Mathematics Subprogram of the Office of Energy Research under contract DE-AC03-76SF00098, and the National Science Foundation and DARPA under grant DMS-8919074.

1 Introduction

In this paper, we complete the development of a level set formulation to simulate deposition, etching, and lithography in integrated circuit fabrication. The goal is an accurate, stable, and efficient technique for surface advancement due to complex motion which, under different physical effects, may include effects of anisotropy, visibility conditions, material-dependent propagation rates, complex sputter laws, re-deposition, re-emission, and surface diffusion. In Part I of this paper, "A Level Set Approach to a Unified Model for Etching, Deposition, and Photolithography I: Two-Dimensional Simulations" [3], the basic equations and algorithms for two dimensional simulations are developed. In Part II, ([4]), the extension to three dimensions was presented, and a large collection of simulations, including three-dimensional etching and deposition into cavities under the effects of visibility, directional and source flux functions, evolution of lithographic profiles, discontinuous etch rates through multiple materials, and non-convex sputter yield flux functions were shown. In [40, 41] the Fast Marching Method was introduced for solving the Eikonal equation which arises in photolithography development simulations. A review of these earlier works, aimed at the micro-electronics community, was presented in [43]. In this paper, we extend these works to fully three-dimensional topographic simulations, including the effects of re-deposition, re-emission, thin films and surface diffusion. This requires the solution of transport equations for arbitrary general surfaces. The validity of various physical models for microfabrication will not be examined. Instead, we hope to provide a robust numerical approach to these phenomena which can then be used to systematically examine various models.

As discussed in [3, 4], a variety of numerical algorithms are available to advance fronts in etching, deposition and photolithography processes. These methods are not unique to such simulations, and in fact are in use in such areas as dendritic growth and solidification, flame/combustion models, and fluid interfaces. They include string methods, cell fraction methods, and characteristic methods. While powerful, these methods have some weaknesses, including difficulties in executing topological change, instabilities near sharp corners and cusps, complexities in three dimensions, lack of robustness issues. Details of these methods are given in [3, 4, 42].

Level set methods, developed by Osher and Sethian in [29], based on the theory and numerics of weak solutions to surface propagation formulated by Sethian [35, 36], offer offer a highly robust and accurate method for tracking interfaces moving under complex motions. They work in any number of space dimensions, handle topological merging and breaking naturally, and are easy to program. They approximate the equations of motion for the underlying propagating surface, which resemble Hamilton-Jacobi equations with parabolic right-hand sides. The central mathematical idea is to view the moving front as a particular level set of a higher dimensional function. In this setting, sharp gradients and cusps form naturally, and the effects of curvature may be easily incorporated. The key numerical idea is to borrow the technology from the numerical solution of hyperbolic conservation laws and transfer these schemes

to the Hamilton-Jacobi setting, which then guarantees that the correct entropy satisfying solution will be obtained. A comprehensive introduction and review of the state-of-the-art of level set methods may be found in [42].

2 Level Set Methods

2.1 The General Level Set Method

Here, we briefly summarize the key ideas behind level set methods; for details, see [29, 38, 42]. Given a moving closed hypersurface $\Gamma(t)$, we wish to produce an Eulerian formulation for the motion of the hypersurface propagating along its normal direction with speed F, where F can be a function of various arguments, including the curvature, normal direction, etc. The main idea is to embed this propagating interface as the zero level set of a higher dimensional function ϕ. Let $\phi(x, t=0)$, where $x \in R^N$ is defined by

$$\phi(x, t=0) = \pm d, \tag{1}$$

where d is the distance from x to $\Gamma(t=0)$, and the plus (minus) sign is chosen if the point x is outside (inside) the initial hypersurface $\Gamma(t=0)$. (Any smooth function will do). Thus, we have an initial function $\phi(x, t=0) : R^N \rightarrow R$ with the property that

$$\Gamma(t=0) = (x | \phi(x, t=0) = 0) \,. \tag{2}$$

Our goal is to now produce an equation for the evolving function $\phi(x, t)$ which contains the embedded motion of $\Gamma(t)$ as the level set $\phi = 0$. Let $x(t), t \in [0, \infty)$ be the path of a point on the propagating front. That is, $x(t=0)$ is a point on the initial front $\Gamma(t=0)$, and $x_t \cdot n = F(x(t))$, where the vector n is normal to the front at $x(t)$. Since the evolving function ϕ is always zero on the propagating hypersurface, we must have

$$\phi(x(t), t) = 0. \tag{3}$$

By the chain rule,

$$\phi_t + \nabla \phi(x(t,t)) \cdot x_t = 0. \tag{4}$$

Since F already gives the speed in the outward normal direction, then $x'(t) \cdot n = F$ where $n = \nabla \phi / |\nabla \phi|$. Thus, we then have the evolution equation for ϕ, namely

$$\phi_t + F|\nabla \phi| = 0 \tag{5}$$

$$\phi(x, t=0) \quad \text{given.} \tag{6}$$

We refer to this as a Hamilton-Jacobi "type" equation because, for certain forms of the speed function F, we obtain the standard Hamilton-Jacobi equation.

In Figure 1, (taken from [37]), we show the outward propagation of an initial curve and the accompanying motion of the level set function ϕ. In Figure 1a, we show the initial circle, and in Figure 1c, we show the circle at a later time. In Figure 1b, we show the initial position of the level set function ϕ, and in Figure 1d, we show this function at a later time.

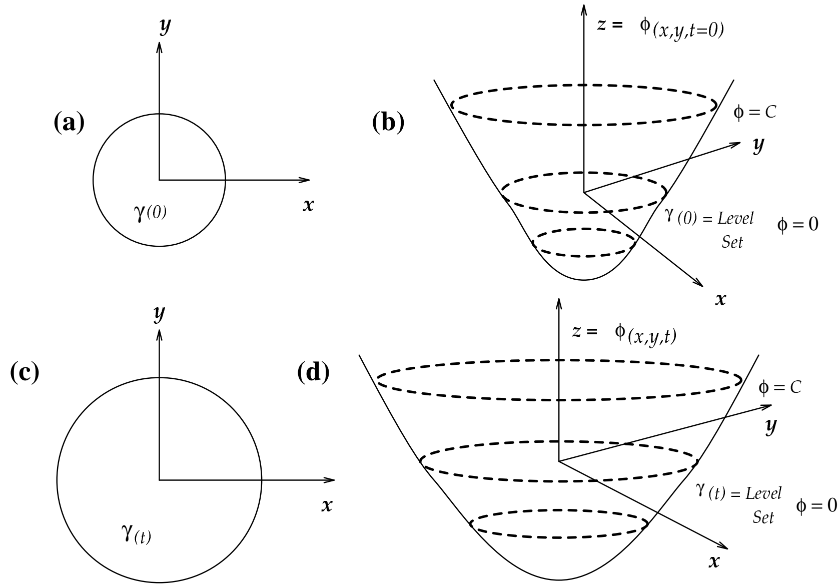

Figure 1: Propagating Circle

The advantages of this approach are well-known. First, the evolving function $\phi(x,t)$ always remains a function as long as F is continuous. However, the level surface $\phi = 0$, and hence the propagating hypersurface $\Gamma(t)$, may change topology, break, merge, and form sharp corners as the function ϕ evolves, see [29]. Second because $\phi(x,t)$ remains a function as it evolves, we may use a discrete grid in the domain of x and substitute conservative upwind finite difference approximations for the spatial and temporal derivatives. Third intrinsic geometric properties of the front, including curvature and normal direction may be easily determined from the level function ϕ. Fourth, there are no significant differences in following fronts in three space dimensions. For details, see [42].

Since its introduction in [29], the above level set approach has been used in a wide collection of problems involving moving interfaces. Some of these applications include the generation of minimal surfaces [12], singularities and geodesics in moving curves and surfaces in [13], flame propagation [32, 48], fluid interfaces [10, 28], shape-from-shading problems [23], shape reconstruction [26] and image processing [24, 25] and fast methods in [2]. The fundamental Eulerian perspective presented by this approach has since been adopted in many theoretical analyses of mean curvature flow, see in particular [16, 11], and related work in [5, 15, 17, 18, 19, 21].

2.2 Fast Narrow Band Methods

Rather than employ the full level set approach, we use a narrow band version which focuses computational labor on cells that bracket the zero level set corresponding to the front. This approach was introduced in [12], used in recovering images in [26], and analyzed extensively in [2]. There are two reasons to do so. The first is speed; in three dimensions, the update count for the full level set method is $O(N^3)$, where N is the number of cells in each direction. By limiting calculations to a narrow band of width k around the zero level set, the operation count drops to $O(kN^2)$, which is a substantial savings. Typically we use bandwidths of 6 cells in each direction, and the corresponding speedup is an order of magnitude over the full level set approach.

The second reason to employ the narrow band construction is because certain properties of the front which contribute to determining its motion have no natural meaning on other level sets. Such variables, known as extension variables, have previously been treated by the following approach; for any given level set, the value of the extension variable is found by using the value on the closest point of the zero level set. For details, see [2], [3]. In this paper, we introduce a new general technique for creating extension velocities.

Local variables, such as normal vectors and curvature have meaning for all the level sets, and may be easily calculated using those values. Normals are calculated using the average one-sided difference technique discussed in [44]. Variations in etch rate, either through masks, material dependence, or lithographic etch rates are directly incorporated into the speed function.

The front is updated using second order in space schemes specially designed for the level set function, see [3, 4, 42]. There are two separate schemes; first, an ENO-based scheme for convex speed functions F which most naturally occur in lithography simulations and some source deposition problems, and a non-convex Lax-Friedrichs/ENO scheme ((see [30]), which can be required for sputter etch/deposition problems. Complete details of these schemes may be found in [3, 4, 42].

3 Equations of Motion for Etching and Deposition

The goal is now to build the speed function F for etching and deposition in the level set framework, namely

$$\phi_t + F|\nabla\phi| = 0 \tag{7}$$

$$\phi(x, t=0) \quad mbox\text{given} \tag{8}$$

Note that F is the speed in the normal direction. Our approach is to write the normal speed function as the superposition of the two main physical effects:

$$F = F_{Etching} + F_{Deposition} \tag{9}$$

The underlying physical effects involved in etching and deposition are quite complex; much of the following summary is obtained from the excellent overviews in [7, 8, 9, 27, 31, 33, 34, 45, 46, 47]. The two effects may be summarized briefly as follows:

- *Deposition:* Particles are deposited on the surface, which causes build-up in the profile. The particles may either isotropically condense from the surroundings (known as chemical or "wet" deposition), or be deposited from a source. In the latter case, we envision particles leaving the source and depositing on the surface; the main advantage of this approach is increased control over the directionality of surface deposition. The rate of deposition, and hence growth of the layer, may depend on source masking, visibility effects between the source and surface point, angle-dependent flux distribution of source particles, and the angle of incidence of the particles relative to the surface normal direction. In addition, particles may not stick, but in fact be re-emitted back into the domain. This is know as "re-emission"; the "sticking coefficient" between zero and one is the fraction of particles that stick. Here, a sticking coefficient of unity means that all particles stick; a low sticking coefficient means that particles may bounce many times before they eventually become fixed to the surface.

- *Etching:* Particles remove material from the evolving profile boundary. The material may be isotropically removed, known again as chemical or "wet" etching, or chipped away through reactive ion etching, also known as "ion milling" Similar to deposition, the main advantage of reactive ion etching is enhanced directionality, which becomes increasingly important as device sizes decrease substantially and etching must proceed in vertical directions without affecting adjacent features. The total etch rate consists of an ion-assisted rate and a purely chemical etch rate due to etching by neutral radicals, which may still have a directional component. As in the above, the total etch rate due to wet and directional milling effects can depend on source masking, visibility effects between the source and surface point, angle-dependent flux distribution of source particles, and the angle of incidence of the particles relative to the surface normal direction. In addition, due to chemical reactions that take place on the surface, etching can cause surface particles to be ejected; this process is known as "re-deposition"; the newly ejected particles are then deposited elsewhere on the front, depending on their angle and distribution.

In the rest of this section, we formalize the above.

3.1 Initial Position and Setup

Define the coordinate system with the x and y axis lying in the plane and z being the vertical axis. We consider a periodic initial profile $h(x, y)$, where h gives the height of the initial surface above the xy plane. We also consider a

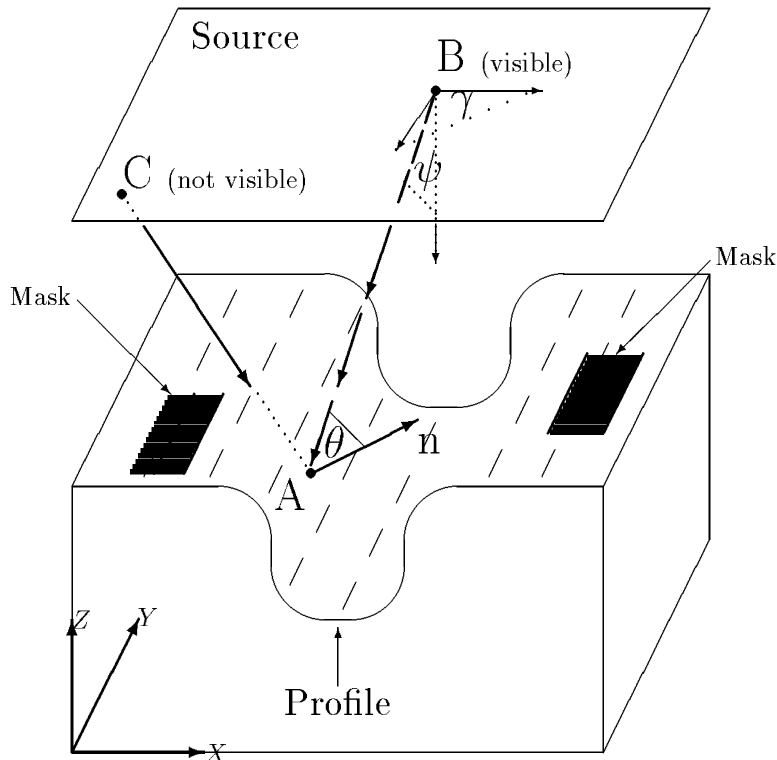

Figure 2: Variables and Setup

source Z given as a surface above the initial profile, and write $Z(x, y)$ referring to the height of the source at the point (x, y).

For both etching and deposition, define the source ray to be the ray leaving the source and aimed towards the surface profile Let ψ be the angle variation in the source ray away from the negative z axis; ψ runs from 0 to π. Let γ be the angle between the projection of the source ray in the xy plane and the positive x axis. Let n be the normal vector at a point x on the surface profile, and θ the angle between the normal and the source ray.

In Figure 2, we indicate these variables. Masks, which force flux rates to be zero, are indicated by heavy dark patches on the initial profile. At each point of the profile, we also assign a visibility indicator function $M_{\Upsilon}(x, x')$ which indicates whether the point x on the initial profile can be seen by the source point x'.

Our goal is to write the effects of deposition, etching, and lithography on the speed F at a point $\vec{x}$ on the front.

3.2 Individual Terms

3.2.1 Etching

We consider two separate types of etching:

- $F_{Isotropic}^{Etching}$: *Isotropic etching.* Uniform etching, also known as chemical or wet etching.
- $F_{Direct}^{Etching}$: *Direct etching.* Etching from an external source; this can be either a collection of point sources, or from an external stream coming from a particular direction. Visibility effects are included; and the flux strength can depend on both the solid angle from the emitting source and the angle between the profile normal and the incoming source direction. Etching can include highly sensitive dependence on angle such as in ion-milling.

3.2.2 Deposition

We consider four separate types of deposition:

- $F_{Isotropic}^{Deposition}$: *Isotropic deposition.* Uniform deposition, also known as chemical or wet deposition.
- $F_{Direct}^{Deposition}$: *Direct deposition.* Deposition from an external source; this can be either a collection of point sources, or from an external stream coming from a particular direction. Visibility effects are included; and the flux strength can depend on both the solid angle from the emitting source and the angle between the profile normal and the incoming source.
- $F_{Re-Deposition}^{Deposition}$: *Re-Deposition.* Particles that are expelled during the etching process. These particles then attach themselves to the profile at other locations; the strength and distribution of the re-deposition flux function can depend on such factors as the local angle. A re-deposition coefficient, $\beta_{re-deposition}$ can range from zero to unity to reflect the fraction of re-deposition that results from the etching process.
- $F_{Re-Emission}^{Deposition}$: *Re-emission deposition.* Particles that are deposited from direct deposition may in fact not stick and are then re-emitted into the domain. The amount of particles re-emitted depends on a sticking coefficient $\beta_{re-emission}$

In Figure 2, we generalize all of these effects as the "source". Thus, the plane source as shown in the figure may consist of locations which emit either uni-directional deposition or point source deposition.

3.3 Assembling the Terms

We may, somewhat abstractly, assemble the above terms into the single expression

$$F = F^{Etching}_{Isotropic} + F^{Etching}_{Direct} + F^{Deposition}_{Isotropic} + F^{Deposition}_{Direct} + F^{Deposition}_{Re-Deposition} + F^{Deposition}_{Re-Emission}. \quad (10)$$

The two isotropic terms are evaluated at a point x by simply evaluating the strengths at that point. The two direct terms are evaluated at a point x on the profile by first computing the visibility to each point of the source, and then evaluating the flux function; thus these terms require computing an integral over the entire source. To compute the fifth term at a point x, we must consider the contributions of every point on the profile to check for re-deposition particles arising from the etching process, thus this term requires computing an integral over the profile itself. The sixth term, $F_{Re-Emission}$ is more problematic; since every point on the front can act as a deposition source of re-emitted particles that do not stick, the total flux function deposition function comes from evaluating an integral equation along the entire profile.

In more detail, let Ω be the set of points on the evolving profile at time t, and let *Source* be the external source. Given two points x and x', let $\Upsilon(x, x')$ be one if the points are visible from one another and zero otherwise. Let r be the distance from x to x', $\vec{n}$ be the unit normal vector at the point x, and finally, let $\vec{\alpha}$ be the unit vector at the point x' on the source pointing towards the point

x on the profile. Then we may refine the above terms as:

$$F = \begin{bmatrix} \text{Flux}_{Isotropic}^{Etching} \\ + \\ \int_{Source} \text{Flux}_{Direct}^{Etching}(r,\psi,\gamma,\theta,x)\Upsilon(x,x')(\vec{n}\cdot\vec{\alpha})dx' \\ + \\ \text{Flux}_{Isotropic}^{Deposition} \\ + \\ \int_{Source} \text{Flux}_{Direct}^{Deposition}(r,\psi,\gamma,\theta,x)\Upsilon(x,x')(\vec{n}\cdot\vec{\alpha})dx' \\ + \\ \int_{\Omega}(1-\beta_{re-deposition})\text{Flux}_{Re-Deposition}^{Deposition}(r,\psi,\gamma,\theta,x)\Upsilon(x,x')(\vec{n}\cdot\vec{\alpha})dx' \\ + \\ \int_{\Omega}(1-\beta_{re-emission})\text{Flux}_{Re-emission}^{Deposition}(r,\psi,\gamma,\theta,x)\Upsilon(x,x')(\vec{n}\cdot\vec{\alpha})dx' \end{bmatrix} \tag{11}$$

The integrals are performed in a straightforward manner. The front is located by constructing the zero level set of ϕ; in two dimensions it is represented by a collection of line segments; in three-dimensions by a collection of voxel elements, see [3, 4]. The centroid of each element is taken as the control point, and the individual flux terms are evaluated at each control point. In the case of the two isotropic terms, the flux is immediately found. In the case of the two integrals over sources, the source is suitably discretized and the contributions summed. In the fifth term, corresponding to re-deposition, the integral over the entire profile is calculated by computing the visibility to all other control points and the corresponding re-deposition term is produced by the effect of direct deposition. Thus, as presented, the fifth term requires N^2 evaluations, where N is the number of control points which approximate the front.

3.4 Evaluation of the Re-emission Term

The sixth and last term is somewhat more time-consuming to evaluate, since the integral requires evaluation of the flux contribution $Flux_{Direct/Re-Deposition}$ from each point of the interface, each of which depends on the contribution from all other points. Thus, this is an integral equation which must be solved to produce the total deposition flux at any point. In the below discussion, we shall assume that the total deposition flux depends on deposition directly from

the source, as well as additional deposition due to particles which do not stick and are in fact re-emitted[1]. We shall call this flux $Flux_{Direct/Re-Deposition}$, and solve for it.

We now introduce some additional notation; in this discussion, we derive the appropriate integral equation for two-dimensional problems; the derivation in three dimensions is similar. Let

- t_i be the coordinates of point number i, with an associated segment length l_i,
- r_{ij} be the distance between point i and j,
- θ^i_j be the angle between the normal to point i and the vector $t_j - t_i$,
- Υ_{ij} be the visibility factor which is one if the point at x_i and x_j can see each other and zero otherwise,
- β_0 be the sticking coefficient for the particles coming directly from the source; $\alpha_0 = 1.0$ means that all the particles stick,
- β be the sticking coefficient for secondary bounces,
- I^i_S be the incoming source strength at point i due to the above light source,
- I^i_R is the source strength at radiated from point i, and
- I_S and I_R be the vectors $(I^0_S, \ldots, I^n_S)$ and $(I^0_R, \ldots, I^n_R)$.

The expression for the the flux is an integral equation for the received flux. Once the problem is discretized into a matrix relation, there are two numerical approaches to solving the equation. The first is to use a direct solver for the matrix equation. In two dimensions, this is practical, for large three dimensional problems this becomes impractical due to the computational labor. The second approach is to construct an iterative solution to the integral equation, based on a series expansion of the interaction matrix. We discuss both approaches below.

3.4.1 Direct Solution of Integral Equation

Our strategy is to first work with the amount I_R radiated from each point of the surface; this depends on the amount received from the direct source plus the amount radiated from all other points on the surface, that is,

$$I^i_R = (1-\beta_0) I^i_S + (1-\beta) \sum_{j, j \neq i} I^j_R \frac{2\cos(\theta^j_i)\cos(\theta^i_j)}{\pi r_{ij}} \Upsilon_{ij} l_j. \tag{12}$$

Define the matrix Ω by

$$\Omega_{ij} = 2\frac{\cos(\theta^i_j)\cos(\theta^j_i)}{\pi r_{ij}} \Upsilon_{ij} l_j, \tag{13}$$

[1]Ion-induced re-deposition particles can be included as part of the re-emission process as well

when $i \neq j$, and 0 if $i = j$.

Note that since $\cos(\theta_j^i) = n_i \cdot \frac{(t_j - t_i)}{|t_j - t_i|}$, Ω can be re-written as

$$\Omega_{ij} = \frac{[n_i \cdot (t_j - t_i)][n_j \cdot (t_i - t_j)]}{\pi |t_j - t_i|^3} \Upsilon_{ij} l_j. \tag{14}$$

Thus,

$$I_R = (1 - \beta_0) I_S + (1 - \beta) \Omega I_R, \tag{15}$$

and we may express I_R in terms of $I + S$ by

$$I_R = (1 - \beta_0)(I - (1 - \beta)\Omega)^{-1} I_S. \tag{16}$$

Thus, the received flux at the front at a point i is given by

$$Flux^i_{DirectDeposition/Re-Deposition} = \beta_0 I_S^i + \beta \sum_{j, j \neq i} I_R^j \frac{2 \cos(\theta_i^j) \cos(\theta_j^i)}{\pi r_{ij}} \Upsilon_{ij} l_j, \tag{17}$$

and, in vector form, we may rewrite this expression as

$$Flux_{DirectDeposition/Re-Deposition} = \beta_0 I_S + \beta \Omega I_R. \tag{18}$$

Our goal now is to eliminate the expression I_R in the above. We first rearrange Eqn. 15 to get

$$\Omega I_R = \frac{1}{(1 - \beta)} I_R - \frac{(1 - \beta_0)}{(1 - \beta)} I_S \tag{19}$$

Substitution into the flux equation (Eqn. 18 then gives

$$Flux_{DirectDeposition/Re-Deposition} = \frac{(\beta_0 - \beta)}{(1 - \beta)} I_S + \frac{\beta}{(1 - \beta)} I_R. \tag{20}$$

Finally, we may substitute the expression for I_R in terms of I_S to get

$$\frac{(\beta_0 - \beta)}{(1 - \beta)} I_S + \frac{\beta (1 - \beta_0)}{(1 - \beta)} (I - (1 - \beta)\Omega)^{-1} I_S. \tag{21}$$

We point out that an important special case is given when $\beta_0 = \beta$ (that is, the sticking coefficient is the same for all bounces), in which case the equation becomes

$$Flux_{DirectDeposition/Re-Deposition} = \beta (I - (1 - \beta)\Omega)^{-1} I_S. \tag{22}$$

We note that in these equations, Ω is non-symmetric.

$$\Psi_{ij} = \frac{n_i \cdot (t_j - t_i) n_j \cdot (t_i - t_j)}{\pi |t_j - t_i|^3} \Upsilon_{ij}, \tag{23}$$

and letting L be the diagonal matrix with $L_{ii} = l_i$, $\Omega = \Psi L$, and Ψ is symmetric. The equation therefore becomes

$$\frac{(\beta - \beta_0)}{(1-\beta)} I_S + \frac{\beta(1-\beta_0)}{(1-\beta)} (I - (1-\beta)\Psi L)^{-1} I_S, \tag{24}$$

$$\frac{(\beta - \beta_0)}{(1-\beta)} I_S + \frac{\beta(1-\beta_0)}{(1-\beta)} L^{-1}(L^{-1} - (1-\beta)\Psi)^{-1} I_S. \tag{25}$$

This matrix is full, and can be quite substantial if the front is complex. We use the symmetric solver in LinPack; approximations to this equation and faster summation techniques will be discussed in later work.

3.4.2 Iterative Solution of Integral Equation

We now consider a different approach, which is to construct an iterative solution to the integral equation, which consists of a series expansion in the interaction matrix. Suitably interpreted, this can be viewed as a "multi-bounce" model, in which the number of terms in the series expansion corresponds to the number of bounces that are particle can undergo before its effects are negligible. This approach will allow us to check the error remainder term in this iterative formulation to determine how many terms must be kept. Since most of the particles either stick or leave the domain after a reasonable number of bounces, this is an effective approach.

We begin by defining the reflected intensity $I_{R,k}$ after the k-th bounce, namely

$$I^i_{R,0} = (1-\beta_0) I^i_S, \tag{26}$$

$$I^i_{R,k+1} = (1-\beta) \sum_{j,j\neq i} I^j_{R,k} \frac{2\cos(\theta^j_i)\cos(\theta^i_j)}{\pi r_{ij}} \Upsilon_{ij} l_j. \tag{27}$$

In a matrix form, this becomes

$$I_{R,0} = (1-\beta_0) I_S, \tag{28}$$

$$I_{R,k+1} = (1-\beta)\Omega I_{R,k}, \tag{29}$$

where Ω is defined as before. Now, define $I_{S,k}$ to be the portion that sticks at the k-th bounce. We then have that

$$I_{S,0} = \beta_0 I_S, \tag{30}$$

$$I_{S,1} = \beta\Omega(1-\beta_0) I_S, \tag{31}$$

and, in general,

$$I_{S,k+1} = \frac{\beta}{1-\beta} I_{R,k+1} = (1-\beta)\Omega I_{S,k}. \tag{32}$$

Therefore, by reaching back to the initial expression, we have

$$I_{S,k} = \beta(1-\beta)^{k-1}(1-\beta_0)\Omega^k I_S, \tag{33}$$

and thus the total intensity after N applications is given by

$$I_N = \beta(1-\beta_0)\left[\sum_{k=1}^{N}(1-\beta)^{k-1}\Omega^k\right] I_S + \beta_0 I_S. \tag{34}$$

Each application of the operator may be viewed as either an additional term in the expansion or an additional included bounce.

We note that there is a recurrence relation for I_N is given by

$$\begin{aligned}
I_{N+1} &= \beta(1-\beta_0)\left[\sum_{k=1}^{N+1}(1-\beta)^{k-1}\Omega^k\right] I_S + \beta_0 I_S \\
&= \beta(1-\beta_0)\left[(1-\beta)\Omega\sum_{k=1}^{N}(1-\beta)^{k-1}\Omega^k + \Omega\right] I_S + \beta_0 I_S \\
&= (1-\beta)\Omega(I_N - \beta_0 I_S) + \beta(1-\beta_0)\Omega I_S + \beta_0 I_S \\
&= (1-\beta)\Omega I_N + (\beta-\beta_0)\Omega I_S + \beta_0 I_S
\end{aligned}$$

By constructing the remainder term $I_{N+1} - I_N$, we can measure the convergence of the expansion and keep enough terms to bound the error below a user-specified tolerance.

4 Additional Numerical Issues

4.1 Constructing Extension Velocity Fields

The above produces the solution to the speed function F at each of the control points x_i. In order to use a level set approximation, an "extension" velocity field (see [42]) must be constructed which provides a velocity field for the neighboring level sets based on F at the control points. One technique is to stand at each grid of the narrow band and simply use the value from the closest point on the front, see [3, 4]. Given a narrow band of radius k, we can find the closest point in $O(k^2)$ in 2D and $O(k^3)$ in 3D. Thus, the total cost for the tube is $O(Nk^3)$ for 2D and $O(N^2k^4)$ in 3D. Another drawback of this method is that away from the front the speed will be discontinuous, which will result in corners and kinks in non-zero level sets.

Here, we introduce a different extension technique based on Sethian's Fast Marching Method for solving the Eikonal equation, which was introduced in [40, 41]. The technique allows one to build an extension velocity field for the general situation in which a velocity must be extended from the front to points within a narrow band, and may be used in a wide collection of applications.

The cost will be $O(Nk \log(N))$ in two dimensions and $O(N^2 k \log(N))$ in three dimensions. As an added benefit, it produces a smooth function off the front. There will still be discontinuities at those grid points where two or more points on the front are the same distance away; however, the stair-stepping exhibited by the previously described pure extension method is not present.

Briefly, the Fast Marching Method is a technique for solving the Eikonal equation

$$|\nabla \phi| F = 1. \tag{35}$$

The technique relies on a combination of narrow band methods, upwind schemes, and a fast sorting algorithm. To imagine an easy case, consider a speed function $F = 1$, thus in this case the goal is to compute the distance function from the initial front. The marching level set method works by propagating the distance values away from the front. At each given time the points being considered are approximately the same distance away from the initial front (give or take a grid cell). When a new point is updated, the values from points with smaller values are used to get a new crossing time. By using a heap sort algorithm, the fast marching method allows one to systematically construct these distance grid values by always marching in upwind fashion, and hence there is never a need to revisit a point once it is updated. If there are N total computational points in the domain, the fast marching method computes the solution to the Eikonal equation in the complete domain in $O(N \log N)$ steps. As such, it is one of the fastest possible techniques for computing the solution to the Eikonal equation. For details, see [40, 41, 42].

To construct an extension velocity field we use a similar idea. The crossing times are found as if the front is advancing with constant speed 1, but rather than only associate distances with each point, we associate distances and extended values with each point. When the crossing time gets updated at a point, its extended value also gets updated, using the extended values of the points that are used to update the crossing time. The simplest method is to use weighted averaging depending on the difference between the new crossing value and the crossing value at the neighboring points.

Algorithmically, we have:

- For the points next to the initial front, specify distance and extension values by using the neighboring points. Extension values are constructed by weighting the nearby values with the distance. These points will be the initial tentative points, and points that lie exactly on the front will be the only accepted points.

- As in the standard fast marching level set technique, pick the smallest tentative crossing time. For each neighboring point that has not been accepted, calculate a new crossing time. This calculation will choose one or two points in two dimensions, and up to three points in three dimensions. Once that crossing time is found, the extension value is set to the weighted average of the extension values from the points used in the crossing time

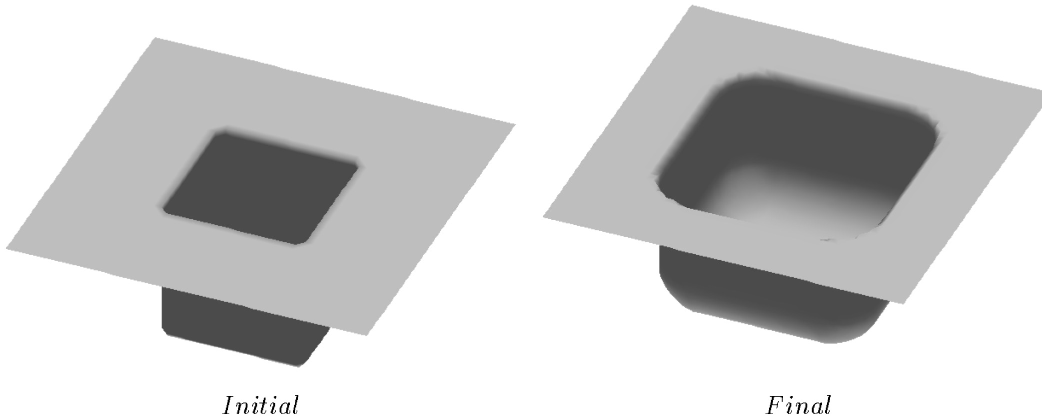

Figure 3: Isotropic Etching into a Hole

calculation. The weight is proportional to the difference between the newly found crossing value and the crossing value at that point.

5 Results

5.1 Basic Calculations

We begin with a straightforward calculation of isotropic etching into a hole, taken from [4]. In Figure 3 we show a square hole from which a material is being isotropically etched; this corresponds to a simple speed function of $F = -1$. As expected, the sides of the cavity are cleanly etched away, leaving smoothed, rounded walls.

We follow with a calculation of source deposition from a plate located above the hole. The effects of visibility and shading are included. Along the entire plate, deposition material is emitted uniformly in each direction. In Figure 4, we show two three-dimensional time plots of the evolving profile. The trench begins to pinch off due to the effects of visibility, and a bulb-shaped profile evolves.

We end the basic calculations section with the modeling (Fig. 5) of the effect of a non-convex sputter etch/ion milling of a saddle surface. The non-convex speed law $F = (1 + 4\sin^2(\theta))\cos\theta$ causes faceting of sharp corners and rounded polishing; for details of this effect, see [4].

5.2 Test Cases: Re-emission/Re-Deposition Simulations

We begin with straightforward studies of etching and re-deposition. In Figure 6, etching occurs under the influence of a uni-directional etching beam coming straight down from the vertical. In Fig. 6a, there is no re-deposition; however, in Fig. 6b, an amount of material equal to the amount etched is re-emitted

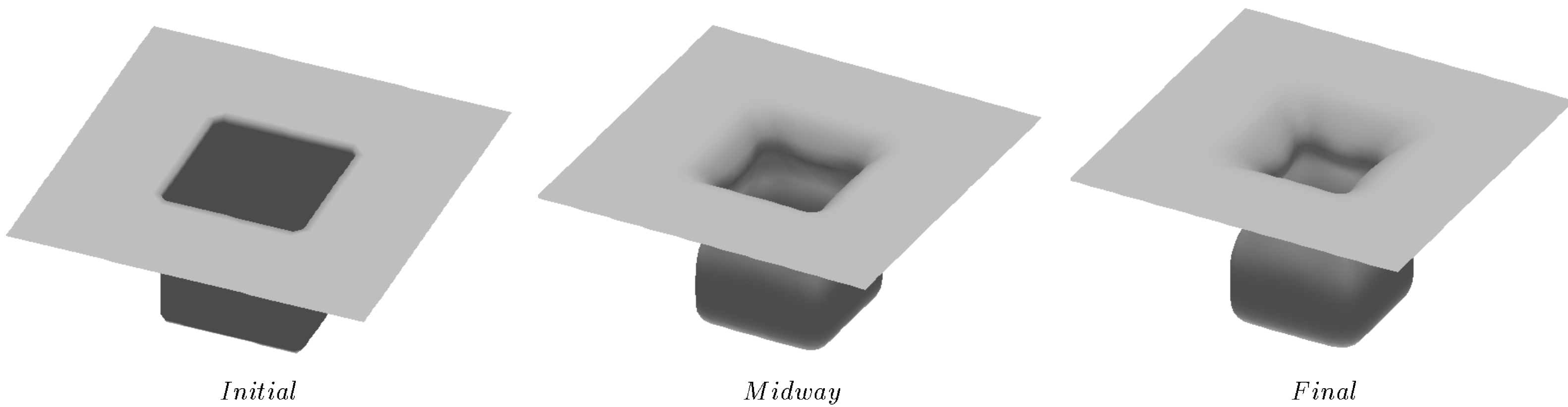

Figure 4: Source Deposition into a Hole

Figure 5: Downward Saddle Under Ion Milling: $F = (1 + 4\sin^2(\theta))\cos\theta$

as a point source at the etching point and re-deposited elsewhere on the front; that is, constant volume is maintained between the etching process and the re-emission process.

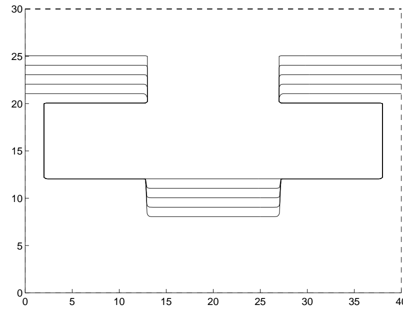

Fig. 6a: Etching

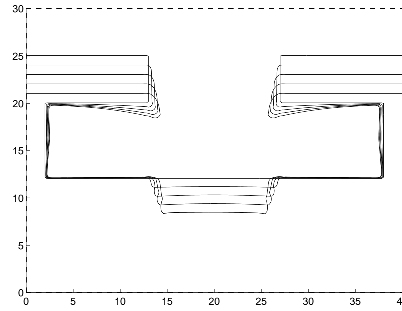

Fig. 6b: Etching plus Re-Deposition

Figure 6: Effect of Re-Deposition on Uni-directional Etching Process

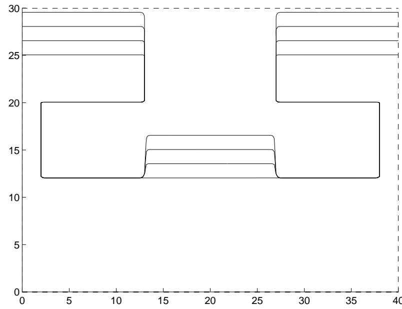

Fig. 7a
Sticking Coefficient 1.0

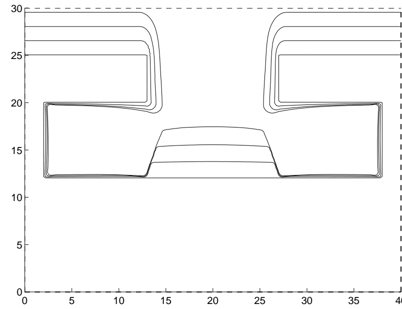

Fig. 7b
Sticking Coefficient .5

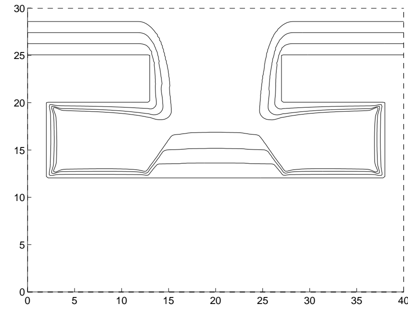

Fig. 7c
Sticking Coefficient .2

Figure 7: Effect of Varying Sticking Coefficient on Deposition/Re-Deposition

Next, we consider a pure deposition process, in which the sticking coefficient is varied. In Figure 7a, a uni-directional deposition beam enters from the vertical, and all of the material sticks (Sticking Coefficient 1.0). In Figure 7b, the sticking is $\beta = .5$, In Figure 7c, the sticking is $\beta = .2$. For sticking coefficient values less than unity, the matrix equation is solved. As the sticking coefficient decreases, the deposition layer becomes more uniformly distributed.

5.3 Complex Examples

We now follow with a collection of more complex simulations designed to demonstrate various physical effects.

5.3.1 Parameter Study

We begin with a two-dimensional parameter study of the simultaneous effects of etching and deposition, without the effects of re-deposition and re-emission. We use a speed function[2]

$$F = (1-\alpha)F_{etch} + \alpha F_{Deposition}, \tag{36}$$

where

$$F_{etch} = (5.2249\cos\theta - 5.5914\cos^2\theta + 1.3665\cos^4\theta), \tag{37}$$

$$F_{Deposition} = \beta F_{Isotropic} + (1-\beta)F_{Source}. \tag{38}$$

As shown in [3, 4], ion-milling terms of this form yield non-convex Hamiltonian-Jacobi equations, and must be computed using appropriate upwind schemes. Visibility effects are considered in all terms except isotropic deposition. The results of varying α and β between 0 and 1 is shown in Figure 8.

5.3.2 Trench Depth on Re-emission Profiles

Next, we study the relationship between body geometry and re-emission profiles. In Figure 9, we show a $3x3$ matrix displaying the interplay between body geometry and various various for the sticking coefficient. We assume a uni-directional deposition beam, and a sticking coefficient of β means that $1-\beta$ of the material is not deposited but instead re-emitted as a point source.

We repeat the study in Figure 10, only this time we assume deposition from a line source above the trench. In both cases, as the depth of the cavity decrease, more re-emission is felt from the bottom of the cavity, and the deposition spread is more uniform. Furthermore, in both cases we observe a slight lagging of the front in corners; this is due to leakage in our discretization of the integral for the front. This problem can be corrected with a non-uniform discretization scheme, which is discussed elsewhere.

[2] This form for the ion-milling term was suggested by J. Rey of Technology Modeling Associates.

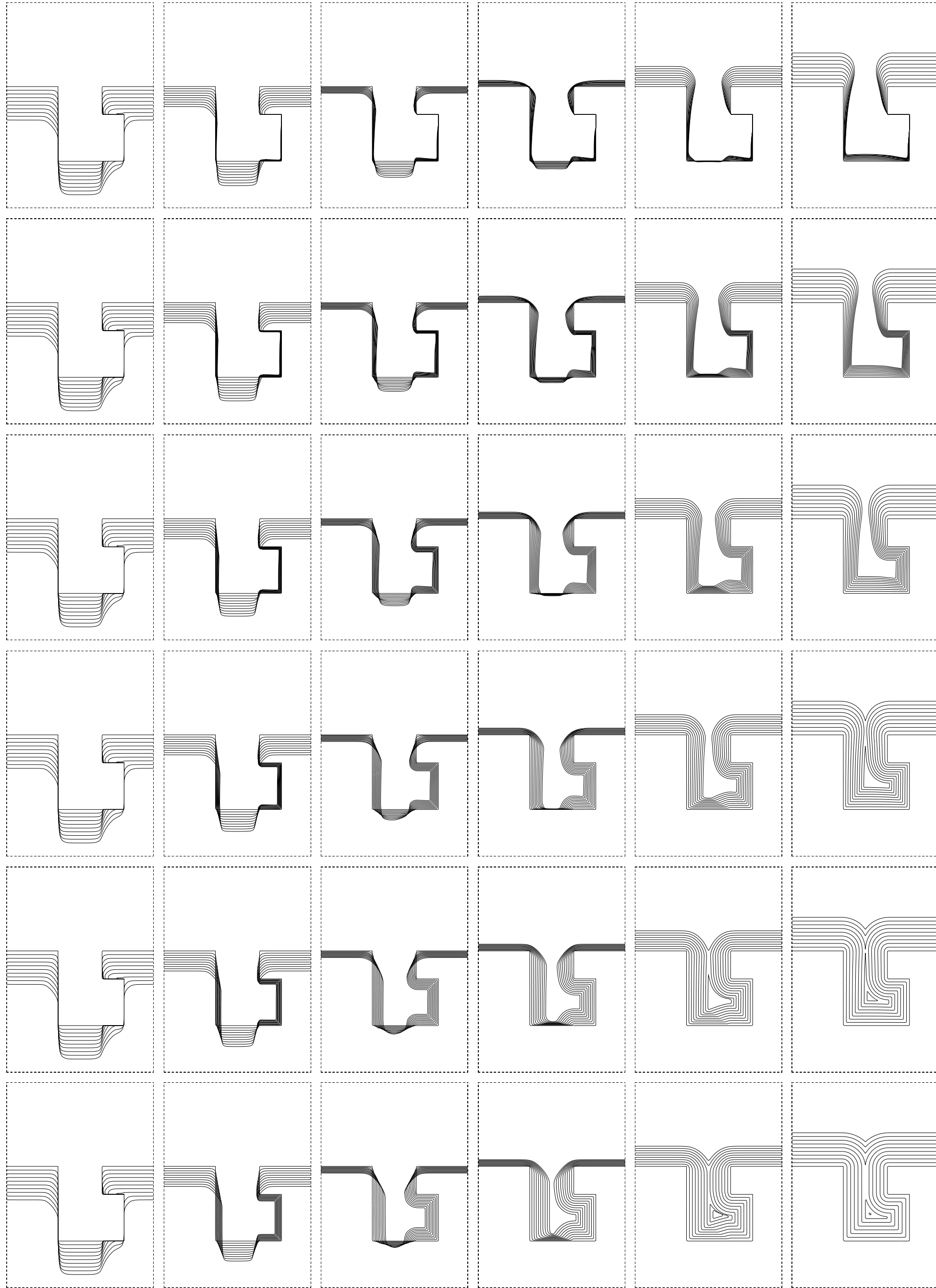

$$F = (1-\alpha)F_{etch} + \alpha F_{Deposition}$$

$$F_{etch} = (5.2249\cos\theta - 5.5914\cos^2\theta + 1.3665\cos^4\theta)\cos\theta$$

$$F_{Deposition} = \beta F_{Isotropic} + (1-\beta)F_{Source}$$

α Increases from left to right
β Increases from top to bottom

Figure 8: Simultaneous etching and deposition

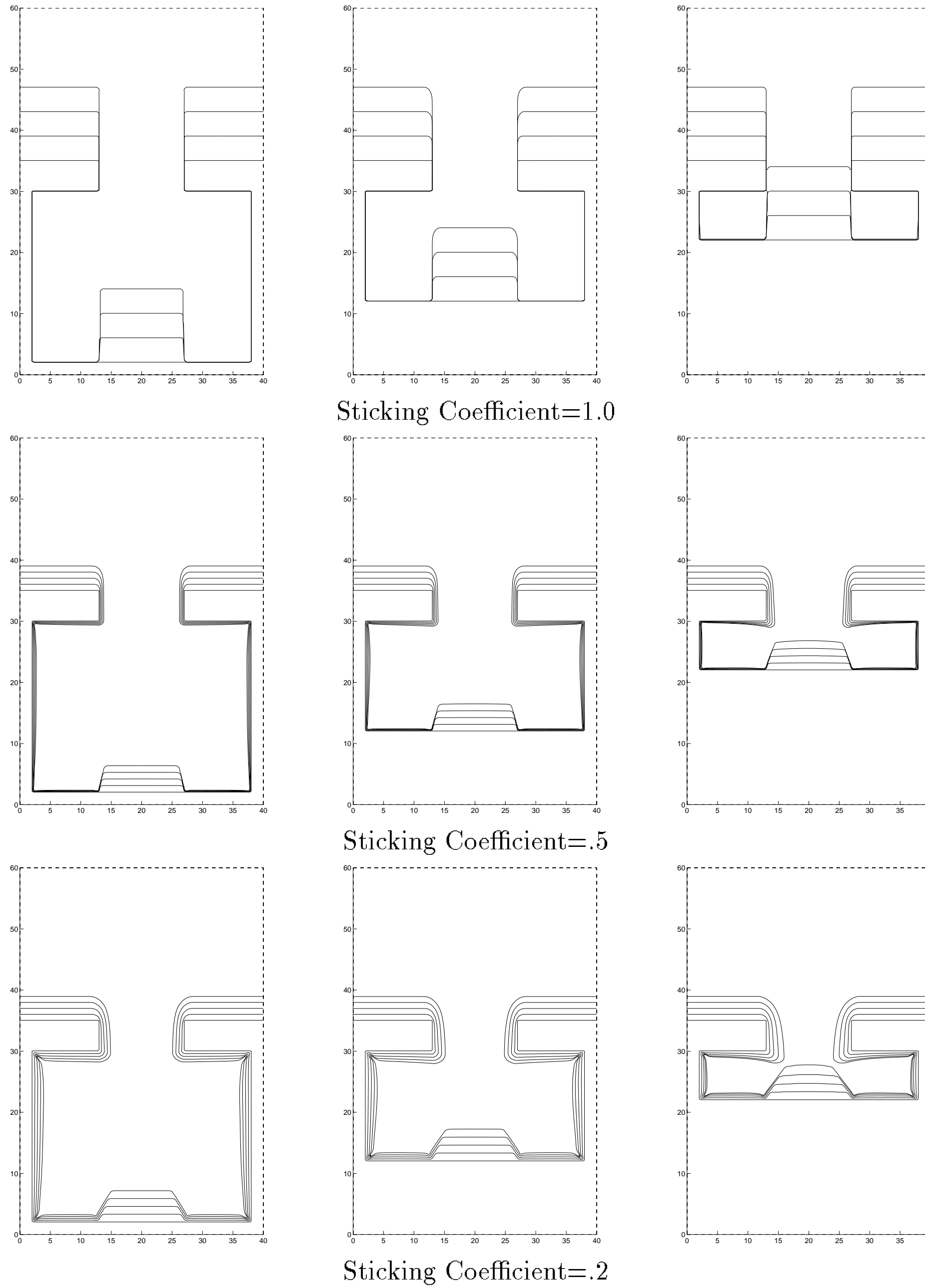

Figure 9: Body Geometry vs. Sticking Coefficient: Uni-directional Deposition

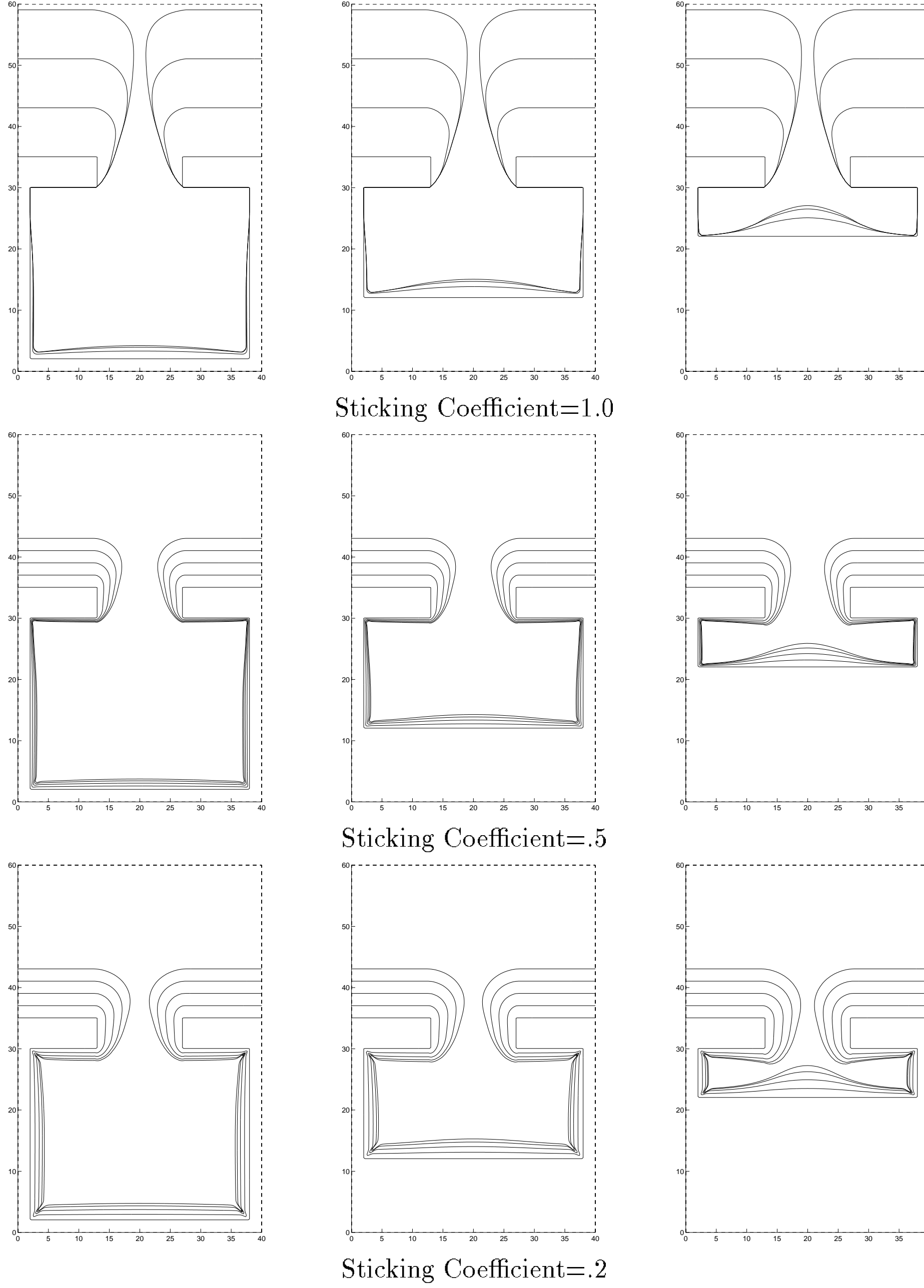

Sticking Coefficient=1.0

Sticking Coefficient=.5

Sticking Coefficient=.2

Figure 10: Body Geometry vs. Sticking Coefficient: Line Source Deposition

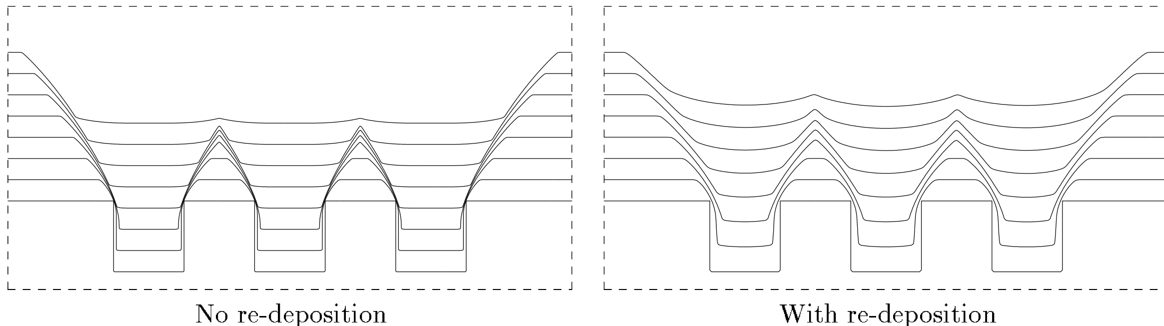

Figure 11: Combination of ion-milling, direct deposition and conformal deposition

5.3.3 Multiple Effects

An important simulation is obtained by considering a periodic sequence of structures under the multiple effects of ion-milling, isotropic deposition, and re-deposition. Here, the goal is to model the faceting that occurs due to the non-convexity of the ion-milling term (see [3, 4]), as well as the role of re-deposition in rounding sharp corners as a function of the re-emission coefficient. A combination of ion-milling and ion-induced sputtered re-deposition are shown in Figure 11, together with conformal deposition and direct deposition. On the left, the ion-induced sputter re-deposition is set to zero, on the right the etched material is re-emitted, producing considerable rounding of the sharp corners.

Next, we consider a complex speed function[3], which consists of a sensitive angle dependent speed law. A plot of the speed as a function of θ shows that for some values of θ, deposition dominates over etching, while for other values, etching is the dominant effect. We further add the restriction that the initial structure is impenetrable and thus cannot be etched. In Figure 12, we show the effect of the speed law

$$F = (4.385 - 5.7\cos\theta + 1.425\cos^3\theta)\cos\theta \tag{39}$$

on a periodic structure. We observe that the impenetrability of the material forces the selection of two critical angles, as seen in the sharp angles at the protruding corners of the structure.

5.3.4 Thin Films/Nanolayers/Triple Points

Next, we consider a problem in which several effects are combined. We imagine an initial block, in which a mask covers a substrate, and envision a simultaneous etch and deposition process. We imagine that one material (which will be shown as light gray)is isotropically deposited on both the mask (shown in dark gray) and substrate (shown in black). At the same time that this material is being

[3]This example was suggested by J. Rey of Technology Modeling Associates

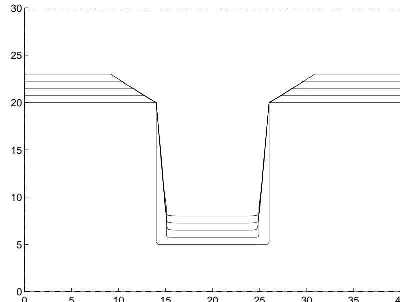

Figure 12: Impenetrable Periodic Block under Simultaneous Etching and Deposition

deposited, it is being etched under an ion-milling/sputter law, such that the etch rate in the substrate is twice as fast as the etch rate in the mask. Thus, we have

$$F = F_{IsotropicDeposition} + F_{SputterEtching} \tag{40}$$

$$F_{IsotropicDeposition} = .5 \qquad F_{SputterEtching} = Factor(x) * \cos\theta \tag{41}$$

- $Factor(x)$= 1.0 if in dark gray material (Mask),
- $Factor(x)$= 2.0 if in black material (Substrate).

In Figure 13, we show the sequence of profile evolution under these effects. We note the development of the thin nano-layer which covers the side walls, but is fully etched away along the top and the bottom; we also note the existence of evolving triple points. We stress out that the grid used for this calculation is significantly larger than the size of the nano-layer; thus our algorithms provide for significant sub-grid resolution without resorting to adaptive mesh technology, see [42] for details of this technology.

We repeat the calculation in Figure 14, only this time using an ion-milling sputter etching speed law which promotes faceting due to the presence of non-convex Hamiltonians; see [3, 4]. Here, we note the rounding of the side wall layers, as well as the existence of triple points and thin layer structures.

5.3.5 Surface Diffusion

Two types of surface diffusion can play important roles in coverage and deposition layers; bulk diffusion, which is the global macro-motion of the material within the deposited layer, and surface diffusion, which relates to the motion

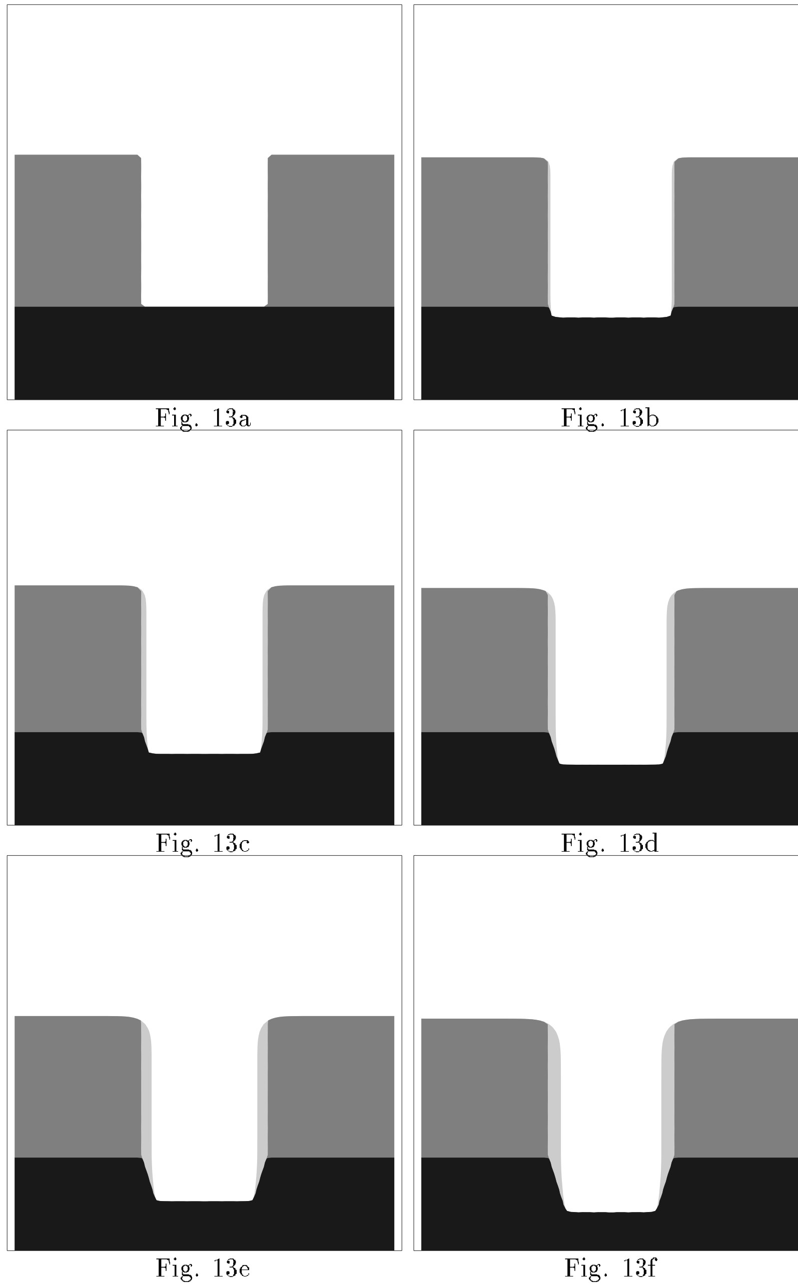

Figure 13: Combination of Isotropic Deposition of Thin Layer and Convex Sputter Etching of Materials: Time Sequence

$$F = F_{IsotropicDeposition} + F_{SputterEtching} \tag{42}$$

$$F_{IsotropicDeposition} = .5 \qquad F_{SputterEtching} = Factor(x) * \cos\theta \tag{43}$$

$Factor(x)$= 1.0 if in Mask (dark gray) / $Factor(x)$= 2.0 if in Substrate(black)

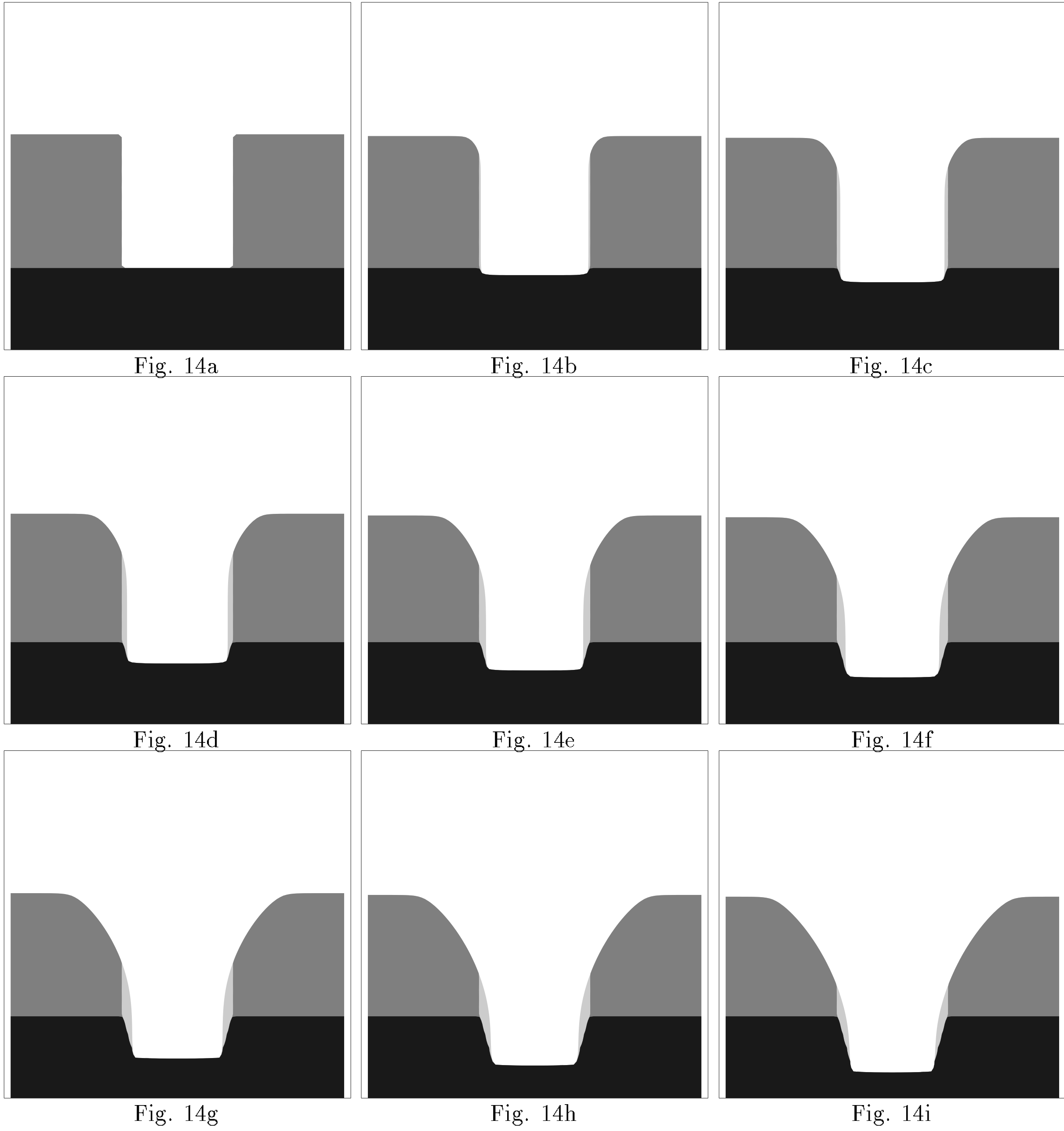

Figure 14: Combination of Isotropic Deposition of Thin Layer and Non-Convex Sputter Etching of Materials: Time Sequence

$$F = F_{IsotropicDeposition} + F_{SputterEtching} \tag{44}$$

$$F_{IsotropicDeposition} = .5 \qquad F_{SputterEtching} = Factor(x) * (1. + 4sin^2\theta)\cos\theta \tag{45}$$

$Factor(x)$= 1.0 if in Mask (dark gray) / $Factor(x)$= 2.0 if in Substrate(black)

of metal boundaries. Here, we examine the effects of surface diffusion on the shape of the deposition layer.[4]

Cale and Jain [6, 22] have performed carefully fit numerical experiments to match experimental evidence of surface diffusion effects of aluminum-(1.5%)copper films. They propose (see Cale and Jain [6], and Cale and Raupp [7, 8, 9]) a model of the form

$$\eta(s) - R(s) + constant\frac{\partial^2 \kappa}{\partial s^2} = 0, \tag{46}$$

where $\eta(s)$ is the ballistic flux of atoms arriving at the surface position s, $R(s)$ is the rate of incorporation of atoms into the solid film, and κ is the signed curvature. We refer the reader to [7, 8, 9] for a detailed discussion of transport equations and related terms.

Here, we analyze a model problem which contains the effects of surface motion driven by surface diffusion. We recall the level set formulation

$$\phi_t + F|\nabla\phi| = 0. \tag{47}$$

A wide collection of problems have been studied when the speed function F is of the form

$$F = 1 - \epsilon\kappa, \tag{48}$$

where κ is the curvature of the interface (see [42]). In the case of surface diffusion, we need to solve a model problem of the form

$$F = 1 + \epsilon\kappa_{\alpha\alpha}, \tag{49}$$

where α is an arc-length parameterization. This is suggestive of the well-known sintering equations, which have been analyzed using a level set formulation by Chopp and Sethian in [14], see also [42]. Briefly, while flow under curvature $F = \kappa$ causes all closed simple curves to become circular, shrink to a point and disappear [20], any circle is stable under motion by the second derivative of curvature $F = \kappa_{\alpha\alpha}$. We know of no formal proofs for limiting states of such curves analogous to the one Grayson proved for motion under curvature [20]. Numerical evidence so far indicates that convex curves become circular and then stop; detailed numerical studies may be found in [14].

The problem is delicate because Eqn. 49 is a time-dependent fourth order partial differential equation, and the presence of the fourth derivative requires an exceedingly small time step for stability in an explicit scheme; the linear fourth order heat equation has a stability time step requirement of the form $O(\Delta t/\Delta h^4)$. Such schemes can in fact be made implicit to allow a larger time step; see [14] for further discussion.

It is tempting to alter the equation and create a surface diffusion model by using a speed function of the form $F(\kappa) = -\epsilon\kappa$, since, for short time, this

[4] We thank T. Cale and J. Rey for illuminating conversations about the role and effects of surface diffusion.

probably gives effects close to the actual sintering equation, and the time step requirement is considerably less drastic. Nonetheless, we have chosen to work with the full fourth order equation.

We can convert the problem to a level set formulation by differentiating the curvature expression twice in the tangent direction along each level line. Following the discussion in [14], we have

$$\phi_t + (1 + \epsilon\kappa_{\alpha\alpha})|\nabla\phi| = 0 \tag{50}$$

$$\phi_t + |\nabla\phi| = -\epsilon\left[\nabla\cdot\frac{\nabla\phi}{|\nabla\phi|}\right]_{\alpha\alpha} \tag{51}$$

$$\phi_t + |\nabla\phi| = -\epsilon\nabla\left[\nabla\left[\nabla\cdot\frac{\nabla\phi}{|\nabla\phi|}\right]\cdot\frac{\phi_y, -\phi_x}{|\nabla\phi|}\right]\cdot\frac{\phi_y, -\phi_x}{|\nabla\phi|} \tag{52}$$

We use a central difference approximation for the derivatives, and regularize the denominator to avoid the singularity associated with vanishing gradients.

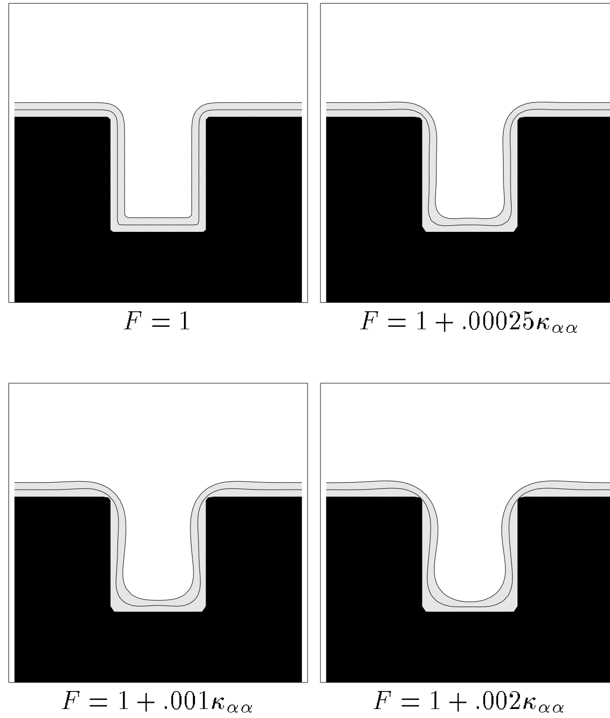

Figure 15: Effects of Surface Diffusion on Isotropic Deposition: $F = 1 - \epsilon\kappa_{\alpha\alpha}$

We begin in Figure 15 by showing the effects of surface diffusion on a model problem of isotropic deposition, that is, we examine a speed function $F = 1 + \epsilon\kappa_{\alpha\alpha}$ for varying values of ϵ.

We next turn to a more realistic case, and consider a speed function which contains isotropic deposition and an ion-milling non-convex etch function together with surface diffusion, that is, in Figure 16 we consider the speed function

$$F = 4 - (1 + 4\sin^2\theta) + \epsilon\kappa_{\alpha\alpha} \tag{53}$$

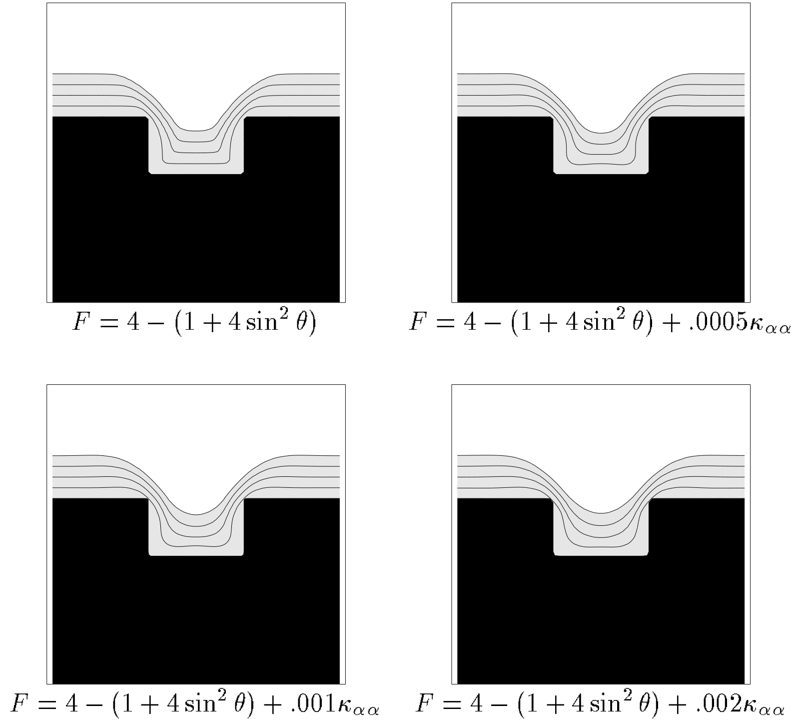

Figure 16: Effects of Surface Diffusion on Deposition Plus Ion-Milling: $F = 4 - (1 + 4\sin^2\theta) + \epsilon\kappa_{\alpha\alpha}$

5.4 Three-Dimensional Effects

Finally, we end with three examples showing three-dimensional problems which includes the effects of a low sticking coefficient on deposition/re-deposition. In Figure 17, we show the effects of a small sticking coefficient on a three-dimensional structure. While the structure is somewhat unrealistic, it is chosen to illustrate the effects under study. The structure is a rectangular trench, with pegs protruding in from opposite sides. In Fig. 17a, we show the initial three-dimensional shape, followed in Fig. 17b by a later configuration. Here, the effect of the deposition is to create a layer everywhere except under the pegs, while the effects of the re-deposition is to create a layer underneath the overhang. Next, in Fig. 17c and Fig. 17d, we show two-dimensional cross-sections of the evolving profile, which better illustrate the effects of the re-deposition.

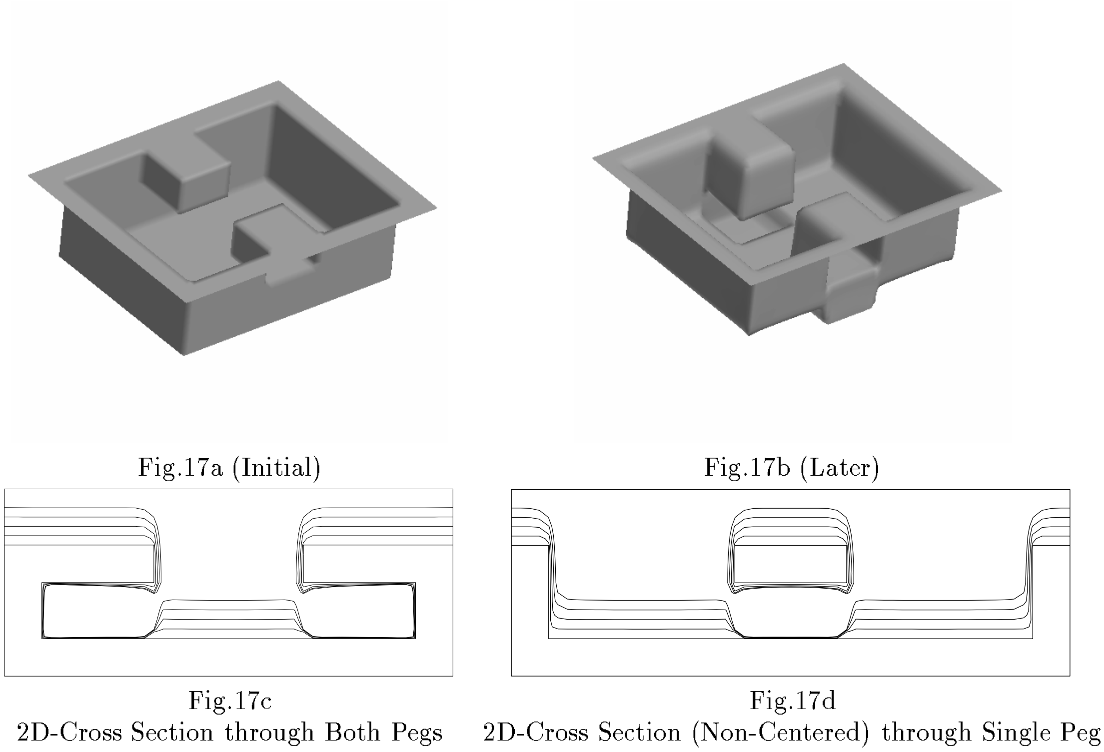

Fig.17a (Initial) Fig.17b (Later)

Fig.17c 2D-Cross Section through Both Pegs

Fig.17d 2D-Cross Section (Non-Centered) through Single Peg

Figure 17: Effects of Low Sticking Coefficient (.1) on 3D Structure

Finally, we perform two studies of complex motions applied to a double-L shape. We begin with a study which balances source distribution with an angular flux cosine dependence with an isotropic deposition term. That is, let the $Flux(x)$ received at a point x on the surface emitted from a point y on the source be given by

$$Flux(x) = .9\cos(\theta_1)\cos(\theta_2) + .1 \tag{54}$$

where θ_1 is the angle that the vector v from x to y makes with the normal at x, and θ_2 is the angle that the vector v makes with the vertical. Figure 18 shows the variables for this expression. This flux is integrated over the entire source to obtain the speed function F at the point x.

In Figure 19, we show the double-L shape under the effects of this flux distribution. Fig. 19a, we show the initial shape from a diagonal angle; the development of a void is clearly shown in the three-dimensional profile shown in Fig. 19b.

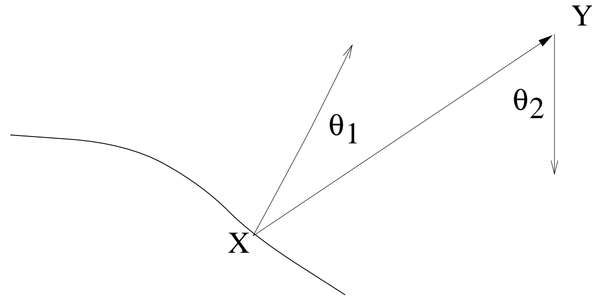

Figure 18: Variables for Double-L Simulations

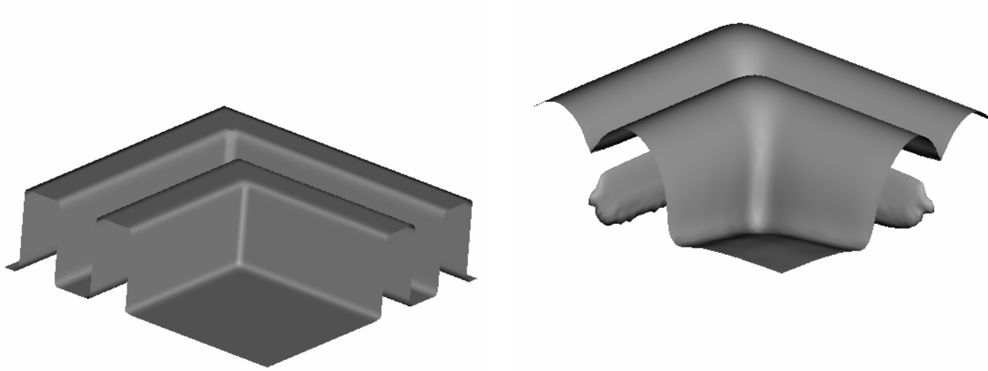

Fig. 19a: Initial Shape

Fig. 19b: Later Time

Figure 19: Three-dimensional Evolution under Cosine Source Distribution and Isotropic Deposition

. .

Finally, in Figure 20, we repeat the calculation using the initial shape shown in Fig. 20a. however, this time we remove the isotropic deposition term, and consider a combination of two cosine flux deposition sources. That is, the initial flux at each point is given by

$$Flux(x) = \cos^5(\theta_1)\cos(\theta_2) + \cos(\theta_1)\cos(\theta_2); \tag{55}$$

in addition, the second deposition term is given a sticking coefficient of .1, thus we also consider the effects of re-deposition. We see that in this case, the void does not form; results are shown after some time evolution in Fig. 20b; a two-dimensional cross-sectional cut is shown in Figure 20c.

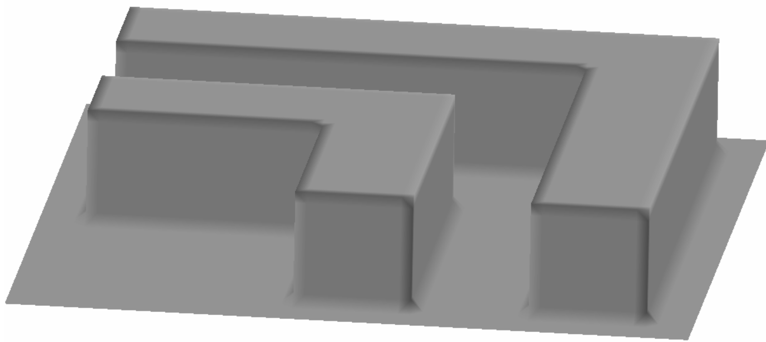

Fig. 20a: Initial Position

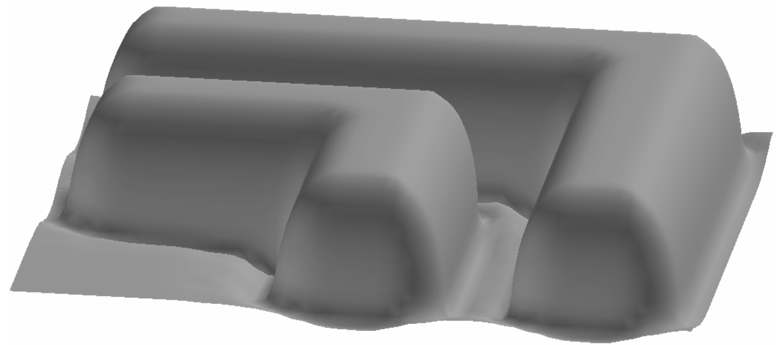

Fig. 20b: Time Evolution

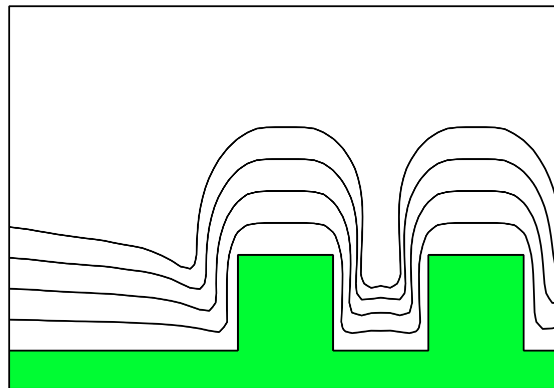

Fig. 20c: 2d Cross-Section

Figure 20: Three-dimensional Evolution under Cosine Source Distribution with Sticking Coefficient .1

. .

6 Timings

The computational labor required in these calculations is most directly a function of the grid resolution required to represent the front and the complexity of the physical effects under consideration. In Figures 21, 22, rough timings are given for various sizes and physical complexities for a Sun Ultra. The lithography timings were computed using the fast marching method given in [41].

Test	50 by 50			100 by 100		
	Runtime	Steps	time/step	Runtime	Steps	time/step
Lithography (Fast Marching)	6.9ms	NA	NA	26ms	NA	NA
Isotropic (Narrow Band)	82ms	24	34ms	0.4s	49	8ms
Unidirectional (with Visibility)	0.4s	17	23ms	2.3s	34	70ms
Etching and Re-Deposition	1.7s	25	68ms	14s	51	0.3s
Deposition and Re-Deposition (Iterative Model)	1.1s	17	65ms	12s	39	0.3s

Figure 21: Two-Dimensional Timings

7 Summary

We have presented in this and previous papers a level set formulation for etching, deposition, and photolithography development simulations. The approach handles a wide collection of complex topographic problems, and provides a unified perspective on these problems. Our next step, currently underway, is to couple this methodology to Navier-Stokes solvers for computing the relevant fluid effects off the front, and to provide hydrodynamic and transport links between the surface evolution and physics in the interior; we shall report on this work elsewhere.

Test	40 by 40 by 40			80 by 80 by 80		
	Runtime	Steps	time/step	Runtime	Steps	time/step
Lithography (Fast Marching)	0.16s	NA	NA	2.1s	NA	NA
Isotropic (Narrow Band)	1.3s	8	0.16s	13.6s	24	0.6s
Unidirectional (with Visibility)	16.7s	24	0.7s	270s	47	5.7s
Etching and Re-Deposition	224s	12	19s	260m	25	10m
Deposition and Re-Deposition (Iterative Model)	265s	11	24s	290m	23	12.6m

Figure 22: Three-Dimensional Timings

Acknowledgements: All calculations were performed at the University of California at Berkeley and the Lawrence Berkeley National Laboratory. A video tape of the above simulations is available by request. We would like to thank L. Borucki, T. Cale, B. Coughran, J. Lee, P. Leon, A. Neureuther, C. Rafferty, J. Rey, V. Singh, K. Smith, and K. Toh for helpful discussions. A web page describing level set methods and this work in particular may be found at http://math.berkeley.edu/~sethian/level_set.html. .

References

[1] Adalsteinsson, D., Kimmel, R., Malladi, R., and Sethian, J.A., *Fast Marching Methods for Computing Solutions to Static Hamilton-Jacobi Equations*, Center for Pure and Applied Mathematics Report, University of California at Berkeley, submitted for publication, SIAM J. Num. Anal,. Feb., 1996.

[2] Adalsteinsson, D., and Sethian, J.A., *A fast level set method for propagating interfaces*, Jour. Comp. Phys., Vol. 118, pp. 269-277, 1995.

[3] Adalsteinsson, D., and Sethian, J.A., *A Level Set Approach to a Unified Model for Etching, Deposition, and Lithography I: Two-Dimensional Simulations*, Vol. 120, No. 1, pp. 128-144, 1995.

[4] Adalsteinsson, D., and Sethian, J.A., *A Level Set Approach to a Unified Model for Etching, Deposition, and Lithography II: Three-Dimensional Simulations*, Vol. 122, No. 2, pp. 348-366, 1995.

[5] Altshuler, S., Angenent, S.B., and Giga, Y., *Mean Curvature Flow through Singularities for Surfaces of Rotation*, preprint, 1993.

[6] Cale, T.S., Jain, M.K., Tracy, C.J., and Duffin, R., submitted for publication, J. Vac. Sci, Tech, B, 1996,

[7] Cale, T.S., and Raupp, G.B., *Free Molecular Transport and Deposition in Cylindrical Features*, J. Vac. Sci. Tech., B, 8, 4, pp. 649–655, 1990.

[8] Cale, T.S., and Raupp, G.B., *Free Molecular Transport and Deposition in Long Rectangular Trenches*, J. Appl. Phys., 68, 7, pp. 3645–3652, 1990.

[9] Cale, T.S., and Raupp, G.B., *A Unified Line-of-Sight Model of Deposition in Rectangular Trenches*, J. Vac. Sci. Tech., B, 8, 6, pp. 1242–1248, 1990.

[10] Chang, Y.C., Hou, T.Y., Merriman, B., and Osher, S.J., *A Level Set Formulation of Eulerian Interface Capturing Methods for Incompressible Fluid Flows*, submitted for publication, Jour. Comp. Phys., 1994.

[11] Chen, Y., Giga, Y., and Goto, S., *Uniqueness and Existence of Viscosity Solutions of Generalized Mean Curvature Flow Equations*, J. Diff. Geom, Vol. 33, 749, 1991.

[12] Chopp, D. L., *Computing minimal surfaces via level set curvature flow*, Journal of Computational Physics, Vol. 106, pp. 77–91, 1993.

[13] Chopp, D.L. and Sethian, J.A., *Flow under Curvature: Singularity Formation, Minimal Surfaces, and Geodesics*, Jour. Exper. Math, 2, No. 4, 1994.

[14] Chopp, D.L., and Sethian, J.A., *A Level Set Approach to the Numerical Simulation of Viscous Sintering*, work in progress, 1996.

[15] Evans, L.C., Sonar, H.M., and Souganidis, P.E., *Phase Transitions and Generalized Motion by Mean Curvature*, Communications on Pure and Applied Mathematics, Vol. 45, 1097, 1992.

[16] Evans, L.C., and Spruck, J., *Motion of Level sets by Mean Curvature*, J. Diff. Geom, Vol. 33, pp. 635-681, 1991.

[17] Evans, L.C., and Spruck, J., *Motion of Level sets by Mean Curvature II*, Transactions of the American Mathematical Society, Vol. 330, 91, 1992.

[18] Falcone, M., Giorgi, T., and Loretti, P., *Level Sets of Viscosity Solutions and Applications*, Instituto per le Applicazioni del Calcolo, Rome, preprint, 1990.

[19] Giga, Y., and Goto, S., *Motion of Hypersurfaces and Geometric Equations*, Journal of the Mathematical Society of Japan, Vol. 44, 99, 1992.

[20] Grayson, M., *The heat equation shrinks embedded plane curves to round points*, J. Diff. Geom., Vol. 26, 285 (1987).

[21] Huisken, G., *Flow by mean curvature of convex surfaces into spheres*, J. Diff. Geom., Vol. 20, 237, (1984).

[22] Jain, M.K., Cale, T.S., Tracy, C.J., and Duffin, R.L., *Curvature Driven Surface Diffusion of Aluminum-(1.5)Copper During Sputter Deposition*, Proceedings, 11th VMIC Conference, 1992.

[23] Kimmel, R., and Bruckstein, A., *Shape from Shading via Level Sets*, Center for Intelligent Systems Report No.9209, Technion- Israel Institute of Technology, June 1992,

[24] R. Malladi and J. A. Sethian, "Image processing via level set curvature flow," *Proc. Natl. Acad. of Sci., USA*, Vol. 92(15), pp. 7046–7050, July 1995.

[25] R. Malladi and J. A. Sethian, "Image Processing: Flows under Min/Max curvature and mean curvature," submitted to *Computer Vision and Image Understanding*, 1995.

[26] Malladi, R., Sethian, J. A., and Vemuri, B. C., *Shape modeling with front propagation: A level set approach*, IEEE Transactions on Pattern Analysis and Machine Intelligence, Vol. 17, No. 2., 1995.

[27] McVittie, J.P.; Rey, J.C.; Bariya, A.J., and others, *SPEEDIE: a profile simulator for etching deposition*, Proceedings of the SPIE - The International Society for Optical Engineering, 1991, vol.1392:126-38.

[28] Mulder, W., Osher, S.J., Sethian, J.A., *Computing Interface Motion in Compressible Gas Dynamics*, Jour. Comp. Phys., Vol. 100, pp. 209-228, 1992.

[29] Osher, S., and Sethian, J. A., *Fronts propagating with curvature dependent speed: Algorithms based on Hamilton-Jacobi formulation*, Jour. Comp. Phys., Vol. 79, pp. 12-49, 1988.

[30] Osher, S., and Shu, C., *High-Order Nonoscillatory Schemes for Hamilton-Jacobi Equations*, Jour. Comp. Phys., Vol. 28, pp. 907-922, 1991.

[31] Rey, J.C.; Lie-Yea Cheng; McVittie, J.P.; Saraswat, K.C., *Monte Carlo low pressure deposition profile simulations*, Journal of Vacuum Science and Technology A (Vacuum, Surfaces, and Films), May-June 1991, vol.9, (no.3, pt.1):1083-7.

[32] Rhee, C., Talbot, L., and Sethian, J.A., *Dynamical Study of a Premixed V flame*, Jour. Fluid Mech., 300, pp. 87-115, 1995.

[33] Scheckler, E.W., Ph.D. Dissertation, EECS, University of California, Berkeley, 1991.

[34] Scheckler, E.W., Toh, K.K.H., Hoffstetter, D.M., and Neureuther, A.R., *3D Lithography, Etching and Deposition Simulation*, Symposium on VLSI Technology, pp. 97-98, Oiso, Japan, (1991)

[35] Sethian, J.A., *An Analysis of Flame Propagation*, Ph.D. Dissertation, Mathematics, University of California, Berkeley, 1982.

[36] Sethian, J.A., *Curvature and the evolution of fronts*, Commun. in Math. Physics, Vol. 101, pp. 487–499, 1985.

[37] Sethian, J.A., *Curvature Flow and Entropy Conditions Applied to Grid Generation*, J. Comp. Phys. Vol. 115, pp.440-454, 1994.

[38] Sethian, J.A., *Numerical algorithms for propagating interfaces: Hamilton-Jacobi equations and conservation laws*, Jour. of Diff. Geom., Vol. 31, pp. 131-161, 1990.

[39] Sethian, J.A., *Numerical methods for propagating fronts*, in Variational methods for free surface interfaces, edited by P. Concus and R. Finn, (Springer-Verlag, New Work, 1987).

[40] Sethian, J.A., *A Review of the Theory, Algorithms, and Applications of Level Set Methods for Propagating Interfaces*, Acta Numerica, 1996.

[41] Sethian, J.A., *A Fast Marching Level Set Method for Monotonically Advancing Fronts*, Proc. Nat. Acad. Sci., 93, 4, 1996.

[42] Sethian, J.A., *Level Set Methods: Evolving Interfaces in Geometry, Fluid Mechanics, Computer Vision and Material Science*, Cambridge University Press, 1996.

[43] Sethian, J.A., and Adalsteinsson, D., *An Overview of Level Set Methods for Etching, Deposition, and Lithography Development*, to appear, IEEE Transactions on Semiconductor Devices, 1996.

[44] Sethian, J.A. and Strain, J.D., *Crystal Growth and Dendritic Solidification* J. Comp. Phys., Vol. 98, pp. 231-253, (1992).

[45] Singh, V.K., Shaqfeh, S.G., and McVittie, J.P., *Simulation of Profile Evolution in Silicon Reactive Ion Etching with Re-emission and Surface Diffusion*, J. Vac. Sci. Tech., B. 10(3), pp. 1091-1104, (1993).

[46] Toh, K.K.H., Ph.D. Dissertation, EECS, University of California, Berkeley, (1990).

[47] Toh, K.K.H., and Neureuther, A.R., *Three-Dimensional Simulation of Optical Lithography,* Proceedings SPIE, Optical/Laser Microlithography IV, vol. 1463, pp. 356-367, (1991).

[48] Zhu, J. and Sethian, J.A., *Projection Methods Coupled to Level Set Interface Techniques* J. Comp. Phys., Vol. 102, pp.128-138, 1992.